Oxidation of Oleic Acid and Oleic Acid/Sodium Chloride(aq) Mixture Droplets with Ozone: Changes of Hygroscopicity and Role of Secondary Reactions

Hui-Ming Hung*,† and Parisa Ariya†,‡

Departments of Atmospheric and Oceanic Sciences and Chemistry, 805 Sherbrooke Street West, Montreal QC H3A 2T5, Canada

The heterogeneous reactions of oleic acid (OL) and oleic-acid/sodium-chloride(aq) (OL/NaCl(aq)) mixture droplets with ozone are studied at two relative humidities (RH). The reactions were monitored concomitantly using attenuated total reflectance Fourier transform infrared spectroscopy (ATR-FT-IR) for the organic species and UV−vis spectrometry for the ozone concentration in order to investigate reaction rate discrepancies reported in literature as well as the oxidation mechanism. The less volatile products were identified and resolved by a Fourier transform ion cyclotron resonance mass spectrometer (FT-ICR-MS). This led to identification of 13 organic molecules (up to 45 carbons). Identified products were predominantly composed by nananoic acid and azelaic acid. Our results suggest that the propagation reaction is possibly initiated by a secondary reaction such as the stabilized Criegee intermediates reacting with oleic acid. For hygroscopic properties, the ATR-IR spectra at high RH (87 ± 5%) showed that the hydrophobic oleic acid droplets can take up water slightly when exposed to ozone. For internally mixed OL/NaCl(aq) droplets, the hygroscopic properties of the droplets upon ozone exposure were found to be complex; hygroscopic properties or the growth factors of the droplets are altered as the oxidation products of oleic acid exist concurrently with NaCl(aq). Furthermore, the concentration of ozone was monitored to examine the kinetics of the oxidation reaction. The integrated ozone profile recorded by UV−vis spectrometry showed the consumed ozone represents only 30 ± 2% of total oleic acid and hence confirmed the existence of secondary reactions. A kinetic model was used to simulate an ozone temporal profile that could only be described if the secondary reactions were included. The discrepancy of ozone uptake coefficients according to the OL and ozone measurements as well as their atmospheric implications are herein discussed.

1. Introduction

Atmospheric particles are abundant in the lower Earth's troposphere, and they can affect life on this planet in several ways such as visibility, health, and climate.[1,2] The influence of the particles is strongly dependent on their chemical compositions and physical properties. For example, the common inorganic compositions, such as sulfate and nitrate, tend to scatter the light, while black carbon absorbs the light, and the chemical compositions with high hygroscopicity tend to have larger size and higher reflection efficiency due to their extra water content.[2,3] However, the chemical composition of the atmospheric particles can vary with time upon reactions with atmospheric oxidants such as gas-phase ozone, hydroxyl radicals, and nitrate radicals,[4−6] which can alter the physical properties of the particles significantly. Over the past few years, oxidation of organic species has received much attention due to their abundance and significant variation in physical properties.

cis-9-Octadecenoic acid (oleic acid, OL) is widely found in atmospheric aerosol phase.[7−12] Sources of this unsaturated fatty acid include the following: naturally, the cell membrane,[9] and anthropogenically, contribution from the process of cooking meat.[11] In several measurements, oleic acid is also present simultaneously with azelaic acid, a possible oxidation product of oleic acid.[8] Because OL is a long-chain carboxylic acid with a double bond, the physical phase of the OL at room temperature is liquid and stable in the condensed phase. Such physical properties make OL a good candidate for the aging study of organic aerosol. Reaction of particle-phase oleic acid with ozone has been extensively studied for in-depth understanding of the chemical processes affecting organic aerosols.[13−21] The overall results show that the physical properties of oleic acid droplets or particles, such as viscosity,[14] hygroscopicity,[14,22] density,[15] and cloud condensation nuclei (CCN) ability,[21] are changed upon exposure to ozone. With the increasing oxygen-to-carbon ratio, the oxidized particles seem to increase their water affinity and facilitate water uptake, becoming larger haze particles.[14,23] The CCN ability of oleic acid is dramatically changed after the oxidation reactions.[21] Among the identified products, in addition to the small molecules such as nonanal and 9-oxo-nonanoic acid at high yields and low yields of azelaic acid and nonanoic acid, several papers support a condensed-phase pathway that leads to formation of products with high molecular weight.[14,20,24−26] Such molecules are believed to arise from reactions of carboxylic acid with stabilized Criegee intermediates, which only occurs in the condensed-phase reactions.[14,20,26] However, there are still some open questions regarding the products and mechanism.

For the reaction of oleic acid with ozone, the literature shows that the ozone uptake coefficients (γ) are not in good agreement with each other, especially for different laboratory set ups. In most oleic-acid-coated flow tube experiments[16,19,27] the loss rate

---

* To whom correspondence should be addressed. E-mail: hm.hung@ mcgill.ca.
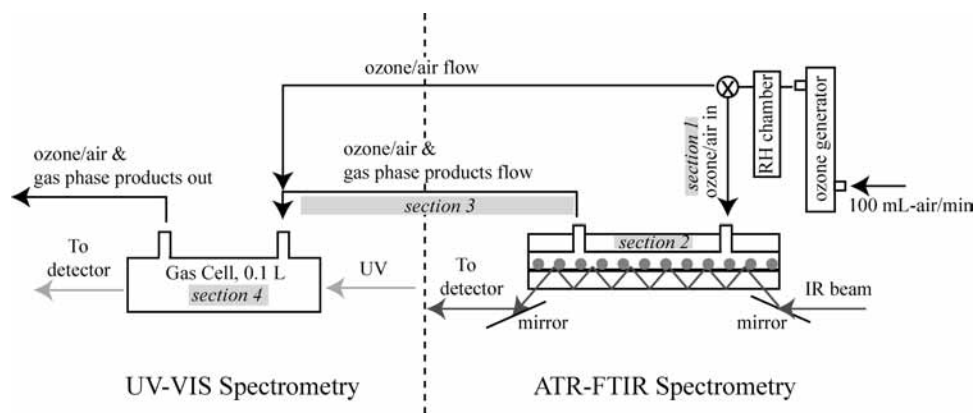† Department of Atmospheric and Oceanic Sciences.
‡ Department of Chemistry.

Figure 1. Schematic diagram of the attenuated total reflectance infrared spectroscopy (ATR-IR) and UV−vis spectroscopy apparatus.

of ozone is monitored and γ is estimated to be $\approx 8 \times 10^{-4}$, while the loss rate of oleic acid is measured in the oleic acid particle experiments with $\gamma \approx (1-10) \times 10^{-3}$.[18,28] Overestimation of the uptake coefficient in the particle experiments is expected to account for losses of oleic acid by other pathways such as addition of stabilized Criegee intermediates to the double bond.[13,14,26] However, the importance of such secondary reactions still requires further evidence.

With the complexity of the aerosol composition in the atmosphere, several groups reported that the oxidation reactions can be affected by the coexisting species. For example, the studies of heterogeneous ozone reaction of internally mixed organic aerosols by Katrib et al.[24] and Knopf et al.[27] show that the oxidation reaction is dependent not only on the composition but also on the physical phase of the particles. In several field measurements the sea-salt aerosols appear to have an organic layer over the sea-salt core.[12,29,30] King et al.[31] shows that the internally mixed OL/NaCl(aq) particles changes size from 6.5 to 8 μm after exposure to ozone at 95% RH by laser Raman tweezers.

In this paper, the heterogeneous ozonolysis of oleic acid and the internal mixture of OL/NaCl(aq) droplets were investigated using attenuated total reflectance infrared spectroscopy (ATR-IR) to understand the impact of organic oxidation on the hygroscopicity of the internally mixed droplets. In order to provide a link between the propagated species with the oxidation mechanism, the less volatile products were analyzed by a Fourier transform ion cyclotron resonance mass spectrometer (FT-ICR-MS), which is a very high-resolution technique to provide masses with very high accuracy. Furthermore, the concentration of both organic species and ozone concentration was monitored in real time concomitantly to investigate the potential discrepancy of uptake coefficients obtained from different laboratories.[16,18,19,27,28] Results from ATR-IR and UV−vis spectrometries were combined to examine the reactions of supported millimeter-sized oleic acid droplets with ozone. In addition to the secondary reactions between stabilized Criegee intermediates and the carboxylic group of oleic acid, the obtained temporal profile of ozone concentration confirms the importance of secondary reaction between stabilized Criegee intermediates and the double bond of oleic acid as proposed by Katrib et al.[26]

2. Experimental Approach

2.1. Preparation of Droplets. The droplets were prepared with a micropipette from either pure oleic acid (>99% purity, Aldrich) or a mixture solution of inorganic saturated aqueous solution with oleic acid blended for 3 min by a cell disruptor (Scientific Industries Inc. Disruptor Genie) just prior to sample dispersion. The droplets were dispersed onto a single-crystal germanium (Ge) surface in the ATR cell (Pike Technologies; 022-5450-500). The ATR cell has a volume of 500 μL. In experiments, 1.5 μL of oleic acid is divided into 12 droplets, previously estimated to have an average horizontal diameter of 2.7 mm and a typical height of 20 μm.[14] The same amount of oleic acid is also dispersed into different numbers of droplets to investigate the possible impact of surface area-to-volume ratio on the ozone temporal profile. However, the surface area-to-volume ratio can only be changed in a small range, so the variation of the ozone temporal profile is not significant.

2.2. Generation of Ozone. Ozone was generated by flowing dry air through either (a) a homemade UV light source which gave a concentration of 20 ppm ozone or (b) the discharged design (model OL100/DC, Ozone Services Inc.) which produced a high concentration of ozone with a partial pressure at least of 500 ppm at 100 mL/min of air flow and 298 ± 2 K. Before entering the relative humidity (RH) chambers, the ozone/air flow passes through a 250 mL empty Erlenmeyer flask to preclude the presence of any oxygen atoms in the flow. The RH chambers are composed of two 250 mL Erlenmeyer flasks, which were filled with 50−100 mL of H_2SO_4 aqueous solution. The RH value of the ozone/air flow was measured using a hygrometer (Panametrics, MC series). The ozone partial pressure in the effluent was monitored using UV−vis spectrometry (Varian Cray 50) with application of Beer's law. An absorbance cross-section of 1.15×10^{-17} cm^2 molecule^{-1} at 254 nm was employed.[2] Ozonolysis of oleic acid was studied by exposing the supported droplets (section 2.1) to 20 or 500 ppm of continuous ozone flow at 298 ± 2 K. With the assumption of the circular cross section for the ATR cell, the 100 mL/min of air flow in the ATR cell is then estimated to have a Reynolds number of ~500, which should not cause any significant turbulence in the cell. However, with the sharp 90° flow direction change from inlet tubing to ATR cell and noncircular cross section of ATR cell, there might be turbulence inside the cell, but it does not cause any significant influence on the droplets as the recorded IR spectra of oleic acid at 100 mL/min of air flow without ozone shows no change with time.

2.3. Analytical Techniques. *2.3.1. Infrared Spectroscopy.* The oxidation reactions of oleic acid droplets with continuous ozone flow were monitored in real time by employing attenuated total reflectance Fourier transform infrared spectroscopy (ATR-FT-IR) (Figure 1). The oleic acid droplets reside on a Ge crystal through which the infrared light propagates. At every reflection the evanescent wave probes the droplets. The penetration depth of the evanescent wave is approximately 6 μm for the Ge crystal. The collected spectra are, therefore, sensitive only to the

622 *J. Phys. Chem. A, Vol. 111, No. 4, 2007*

Hung and Ariya

TABLE 1: Volume and Initial Concentration of Ozone at High Ozone Dose for Individual Section

section	volume (mL)	$A_{254nm,i}$
1	2	0
2	0.5	0
3	3.2	0
4	90	1.56 ± 0.04

condensed-phase reaction products and not to any volatilized reaction products. The infrared absorbance spectra are collected using a Bomem FT-IR (MB series) set to a resolution of 4 cm^{-1}, a spectral range of 700−4000 cm^{-1}, with an averaging of 10 scans. A clean Ge crystal is used for the background spectrum. Reference infrared spectra for products such as nonanoic acid, 1-nonanal, azelaic acid, 9-oxononanoic acid, and azelaic acid monomethyl ester were obtained from Hung et al.[14]

2.3.2. UV−vis Spectroscopy. The ozone concentration was monitored using UV−vis spectrometry. The initial ozone concentration was determined as the flow direction was controlled by a three-way valve to bypass the ATR cell. After the initial ozone concentration was recorded, the ozone flow was then switched to pass the ATR cell to oxidize the oleic acid droplets. The scan rate was 12 scans min^{-1}. With its high signal-to-noise ratio, the absorbance of ozone at 500 ppm is the case used in the modeling analysis. The contribution of the volatile organic products to the absorbance at 254 nm is assumed to be negligible in this study. When the ozone concentration is reduced to 20 ppm, the signal-to-noise ratio is significantly reduced and the absorbance data can only provide qualitative information.

2.3.3. Mass Spectrometry. The products of oleic acid oxidation have been studied extensively.[14,20,26,32] In this study, the observed propagated molecules were analyzed using a Fourier transform ion cyclotron resonance mass spectrometer (FT-ICR-MS, IonSpec 7.0 Tesla, Lake Forest, CA) equipped with electrospray ionization. Two samples were analyzed for the product information: (1) the sample collected from the Ge crystal after 90 min oxidation and (2) 30 μL of oleic acid directly dispersed into droplets on the wall of a 10 mL vial and then exposed to 500 ppm ozone for 100 min. The droplets in sample 2 were larger than sample 1 due to the cohesion of oleic acid droplets to form 2 or 3 droplets inside the vial. The droplets were then dissolved in acetonitrile/water or methanol/water solution for further analysis. The FT-ICR-MS for the two cases were similar except that some residual oleic acid was observed for sample 2. Due to the different ionization efficiency for different mass ranges, this mass analysis only provides qualitative information for the product species. Collision-induced-decomposition (CID) technique was applied to a select parent ion to yield structurally informative fragments. The instrument resolution for this study is at least 20 000 for 1000 amu mass.

2.4. Model Methodology. A kinetic model is applied to simulate the ozone absorbance at 254 nm recorded in UV−vis spectrometry. For simplification, the system from ozone/air inlet to the UV cell is divided into four sections as shown in Figure 1. Section 1 is the tubing connection from the three-way valve to the inlet of ATR cell, section 2 is the ATR cell, section 3 is the tubing connection from the outlet of ATR cell to the inlet of the Quartz cell, and section 4 is the Quartz cell. The volume and initial concentration of ozone for individual sections at the 500 ppm ozone dose are listed in Table 1. Due to the small volume for sections 1−3, the ozone concentration is assumed to be well mixed, so the variation of ozone partial pressure for sections 1−3 can be expressed by the following equations

Section 1: $\quad \dfrac{dP_{O3,1}[t]}{dt} = \dfrac{v_f}{V_1}(P_{O3,0} - P_{O3,1}[t])$ (1)

Section 2:

$$\dfrac{dP_{O3,2}[t]}{dt} = \dfrac{v_f}{V_2}(P_{O3,1}[t] - P_{O3,2}[t]) -$$

$$\text{oxidation reactions} \quad (2)$$

Section 3: $\quad \dfrac{dP_{O3,3}[t]}{dt} = \dfrac{v_f}{V_3}(P_{O3,2}[t] - P_{O3,3}[t])$ (3)

where $P_{O3,i}$ and V_i are the outlet ozone concentration and volume at section i and v_f is the flow rate (100 mL/min in this study). The oxidation reactions in eq 2 are adapted by the proposed mechanism as discussed in section 3.4.1. Since the system was constructed with Teflon tubing and stainless steel connections, we assumed there was no significant ozone uptake by the walls except the chemical reaction given in section 2. The recorded absorbance in UV−vis spectrometry is the concentration in section 4, which is the integration over the whole UV cell based on the outlet ozone flow obtained from section 3. Under such assumptions the ozone partial pressure for section 4 is estimated by the following equation

Section 4: $\quad P_{O3,obs}[t] =$

$$\int_{t-(V_4/v_f)}^{t}(\text{UnitStep}[-t]P_{O3,0} + \text{UnitStep}[t]P_{O3,3}[t])\,dt \quad (4)$$

where UnitStept is a unit step function of time. With the proposed oxidation mechanism applied to eq 2, $P_{O3,obs}[t]$ is then calculated and compared with recorded intensity.

3. Results and Discussion

Changes in the water content of oleic acid after reactions with ozone at RH = 87 ± 5% and the effect of the oleic acid oxidation on the liquid water content of NaCl(aq) are presented in sections 3.1 and 3.2, respectively. The mass spectrometry analysis for less volatile products and the concentration profile of ozone as a function of reaction time are subsequently presented in sections 3.3 and 3.4.

3.1. Hygroscopic Properties of Oleic Acid Droplets upon Reacting with Ozone. IR spectra of the oxidation of oleic acid droplets are shown in Figure 2 for an ozone concentration of 20 ppm. The RH was controlled at 87 ± 5% most of time except for the time period between 170 and 175 min when RH was reduced to 10 ± 3% to show the influence of RH on IR spectra. The temporal responses for several IR regions, such as C−O and C−C stretching, H$_2$O bending, and two different types of C=O stretching modes (acid and ester), are shown in Figure 3. When the droplets are exposed to ozone, the increased absorbance of water bending peak at wavenumber (ν) of 1630 cm^{-1} indicates that the water affinity of the droplets is changed after oxidation reactions. Although the peak intensity is weak, the response to RH variation suggests the existence of liquid water. A similar response to RH variation is also observed at ν = 3400 cm^{-1}, corresponding to OH/OOH stretching (temporal profile not shown), but the intensity is only reduced to one-half as the RH is reduced to 10 ± 3% due to the remaining contribution of OOH from the products. The small water peak observed in this study can only indicate that the droplets allow the water vapor to condense on them when the oxidation reaction happens. As compared to other studies such as Hung et al.,[14] Asad et al.,[22] and Broekhuizen et al.,[21] the 87 ± 5% of RH applied in this study is not high enough to deliquesce the whole droplet.

Oxidation of OL/NaCl(aq) Mixture Droplets with Ozone

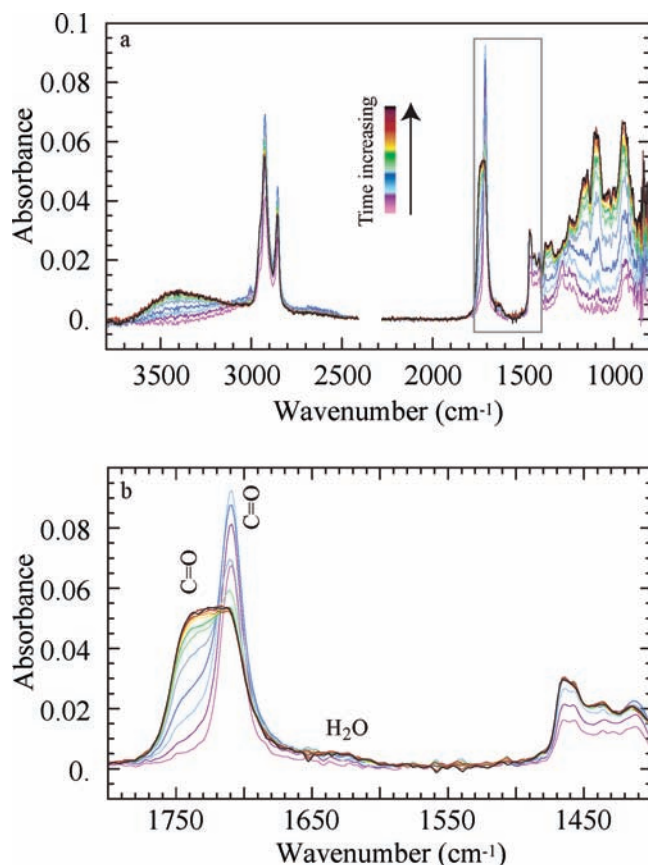*J. Phys. Chem. A, Vol. 111, No. 4, 2007* **623**

Figure 2. Spectral changes with ozone exposure of oleic acid droplets. (a) IR spectra of oleic acid droplets as exposure to ozone/air from $t = 0$ to 240 min. (b) Expanded data for C=O groups at $1675-1800$ cm^{-1} and water bending peak over 1680 cm^{-1}. Conditions: 20 ppm O$_3$, 100 mL/min of air flow, 1 atm, 298 K, 87 $\pm$ 5% RH, and 2.7 mm droplets.

However, the wet surface might significantly promote hydrolysis reactions in the atmosphere, such as the hydrolysis of N$_2$O$_5$. The small oscillation (± 0.00025) of the water peak at ozone exposure times longer than 50 min might be due to slight water vapor fluctuation inside the spectrometer and thus has no influence on our conclusion.

Without considering the RH variation between 170 and 175 min, the temporal responses for most functional groups shown in Figure 3 increase monotonically with ozone exposure time except the carboxylic C=O stretching frequency at 1706 cm^{-1} $< \nu < 1714$ cm^{-1}, which increases with ozone exposure time for the initial reaction and then decreases afterward. The trend of C=O groups is consistent with the study by Hung et al.[14] and also observed at RH = 10 $\pm$ 3% in this study. In the temporal profile, the water peak has a faster response to the oxidation reaction according to the rate constant of the exponential fitting in Figure 3. This result is possibly due to the difference in hygroscopicity response at different oxidation time. As water deposits onto the OL droplets, the oxidation process might be altered. However, the kinetic data at low and high RH show no significant difference in this study. This suggests that the effect of RH and the deposited liquid water on the oxidation kinetic process might be negligible, at least for this study. When the RH is reduced to 10 $\pm$ 3% at ozone exposure times of $170-175$ min, the intensity of the water peak at $\nu = 1630$ cm^{-1} nearly disappeared (Figure 3c) while the intensity of C=O peaks was higher, as shown in Figure 3d and 3e. Conversely, there is no significant effect on the absorbance for C–O (1103 cm^{-1} $< \nu < 1115$ cm^{-1}) and C–C (1155 cm^{-1} $< \nu < 1189$ cm^{-1}) when RH is reduced. The results from RH
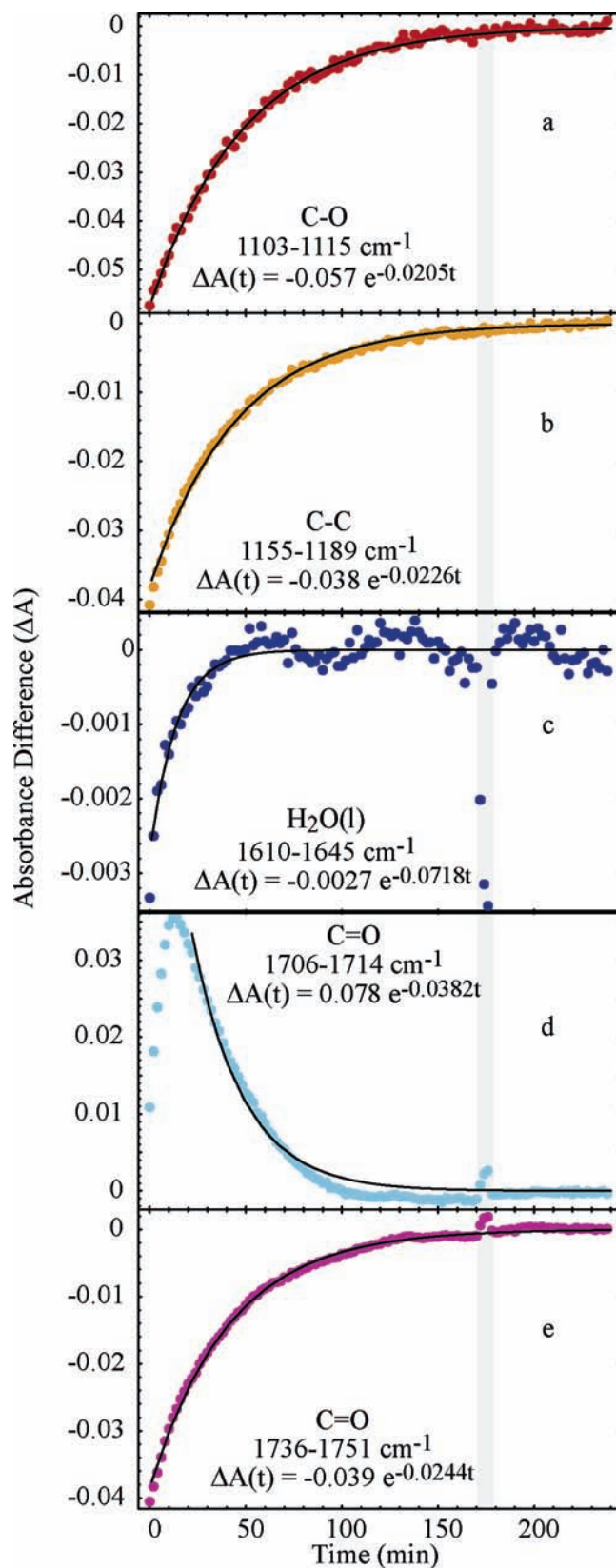

Figure 3. Temporal response for several regions of the infrared spectra shown in Figure 2. The RH is controlled at 87 $\pm$ 5% except the gray region for the time period between 170 and 175 min when RH was reduced to 10 $\pm$ 3%. Results are fit to exponential functions $\Delta A(t) = Be^{-kt}$ (solid black line), where B is the relative absorbance difference and k is the first-order rate coefficient. Conditions: same as Figure 2.

variation indicate that the interaction between water molecule with C=O groups might be more significant than that of water with C–O or C–C groups. Such results suggest that the C–O
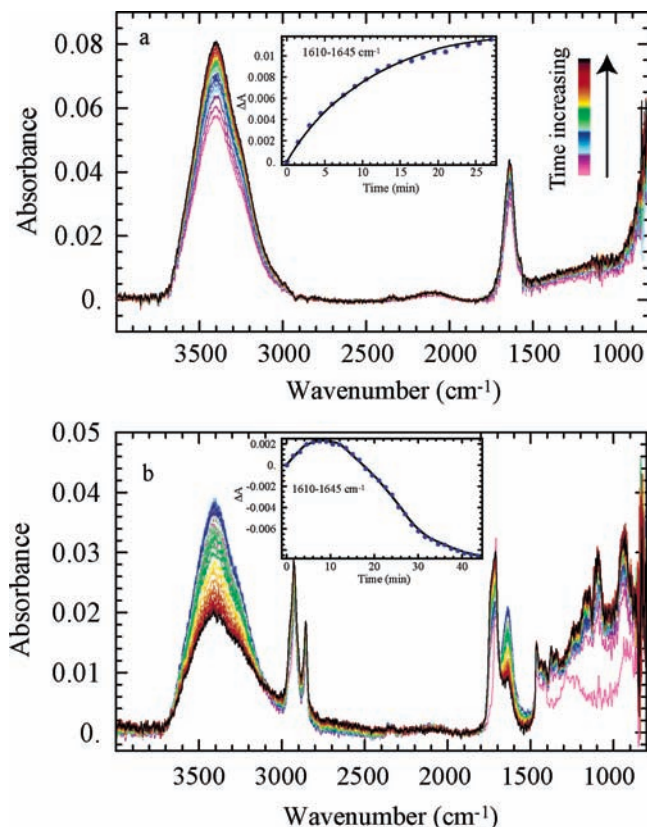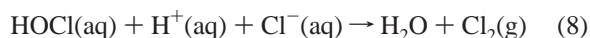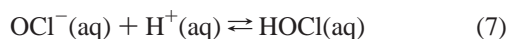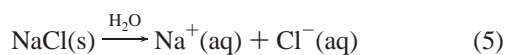
Figure 4. Infrared spectra recorded during O_3 exposure for two types of droplets: (a) NaCl(aq) and (b) OL/NaCl(aq). Conditions: 500 ppm O_3, 100 mL/min of air flow, 1 atm, 298 K, 87 ± 5% RH, and 2.7 mm droplets.

and C—C frequencies present in this study are likely to be part of the nonpolar groups, depicting less water affinity.

3.2. Effect of Oleic Acid Oxidation to Liquid Water Content of NaCl(aq). Figure 4a and 4b shows the IR spectra of NaCl(aq) and internally mixed oleic-acid/NaCl(aq) droplets exposed to ozone at RH = 87 ± 5%, respectively. Since there is no significant absorbance for NaCl at $\nu = 700-4000$ cm^{-1}, the two broad peaks in Figure 4a are mainly contributed by the aqueous water. When the NaCl(aq) droplets were exposed to ozone, the intensity of water peaks increased monotonically with ozone exposure time. The temporal profile of the water bending peak at $\nu = 1630$ cm^{-1} with ozone exposure time is shown in the insert plot of Figure 4a. The increased liquid water content can be potentially due to the following chemical reactions between NaCl(aq) with ozone[33]

$$NaCl(s) \xrightarrow{H_2O} Na^+(aq) + Cl^-(aq) \tag{5}$$

$$Cl^-(aq) + O_3(g) \rightarrow OCl^-(aq) + O_2(g) \tag{6}$$

$$OCl^-(aq) + H^+(aq) \rightleftharpoons HOCl(aq) \tag{7}$$

$$HOCl(aq) + H^+(aq) + Cl^-(aq) \rightarrow H_2O + Cl_2(g) \tag{8}$$

For NaCl in the aqueous phase the reaction is initiated by the dissociated chloride ion with ozone to form OCl$^-$. The rate constant for reaction 6 is less than 3×10^{-3} M^{-1} s^{-1}.[33] OCl$^-$ is then in equilibrium with HOCl, which can further react with chloride to form Cl$_2$. During the reaction HOCl and Cl$_2$ might escape from the droplets and the droplets can become more basic due to the consuming of H$^+$ in both reactions 7 and 8. The IR

spectra in Figure 4a cannot distinguish the contribution of HOCl (or OCl$^-$) because reaction 6 is very slow and the absorbance of H$_2$O—HOCl overlaps with H$_2$O.[34] For a given RH, the new chemical composition can have different liquid water contents as compared to NaCl. The observed increase in the water signal with ozone exposure time suggests the following two possibilities: (1) the composition after exposure to ozone tends to have higher water content than NaCl at the same RH and/or (2) the droplets become more flat which increases the contact surface of liquid water with Ge crystal as the oxidation reaction happens.

For the internal mixture of oleic acid with saturated NaCl aqueous solution (OL/NaCl droplets), the hydrophobic oleic acid molecule tends to form a coating layer outside of the droplets and possibly inhibits NaCl from taking up water. This suggestion is supported by the lack of increase in the water IR absorption for OL/NaCl droplets when the RH is increased from 75% to 87 ± 5%. However, as OL/NaCl(aq) droplets are exposed to ozone, the water content increases with ozone exposure time for the initial 10 min and then decreases subsequently (Figure 4b). With the comparable magnitude to the increased water intensity between Figure 4b and Figure 3, the increasing liquid water content might be related to water uptake by the products from the ozonolysis of OL. It is also possible that ozone diffuses into the droplet and reacts with NaCl(aq), leading to a higher water content via reactions 5−8. As the oleic acid droplets are exposed to enough ozone doses the products formed from the oxidation reaction might mix with the aqueous part of the droplets, which have different hygroscopicity according to observation. The overall liquid water content of the OL/NaCl-(aq) droplets after ozone reaction thus decreases at RH = 87 ± 5%. At the same time, the enhanced organic IR signal indicates that the contact surface area between the organic matters with Ge crystal increases. Overall, the results suggest that the mixture of the products from oleic acid oxidation with NaCl lead to either a higher deliquesce RH or a lower growth factor.

Since droplet size and the contact surface with Ge crystal varied during the oxidation reaction, the chemical kinetics of the OL oxidation cannot be resolved in this study. However, the ATR-IR spectra show a strong similarity in the products with or without liquid water present. This indicates the effect of liquid water on the oxidation of oleic acid might not be significant in the current system but still should not be ruled out. Further investigation of this aspect might be required using other suitable techniques.

3.3. Products and Mechanism of the Ozonolysis of Oleic Acid. Several condensed-phase products such as 1-nonanal, 9-oxononanoic acid, nonanoic acid, and octanoic acid have been identified by GC-MS, while azelaic acid, 9-oxononanoic acid, and other unidentified species that have mass weight up to 1039 amu were found using LC-MS in the similar droplet system.[14] For LC-MS spectra, the unidentified high-mass species were proposed generated by polymerization occurring during the ozonolysis of oleic acid droplets, but there are still some open questions regarding the products and mechanism. In this study, the high-mass species were analyzed to provide evidence for a polymerization mechanism which has been also partially suggested by the study of Ziemann.[20]

The FT-ICR-MS mass spectra are summarized in Figure 5 including two mass spectra with different scanning mass range and two CID mass spectra. FT-ICR-MS provides a highly accurate mass-to-charge ratio along with high-resolution measurements, permitting precise determination of the chemical formula. For instance, the peak at 565 amu of low mass accuracy spectrometry can be assigned as $C_{27}H_{49}O_{12}^+$, a combination of

Oxidation of OL/NaCl(aq) Mixture Droplets with Ozone
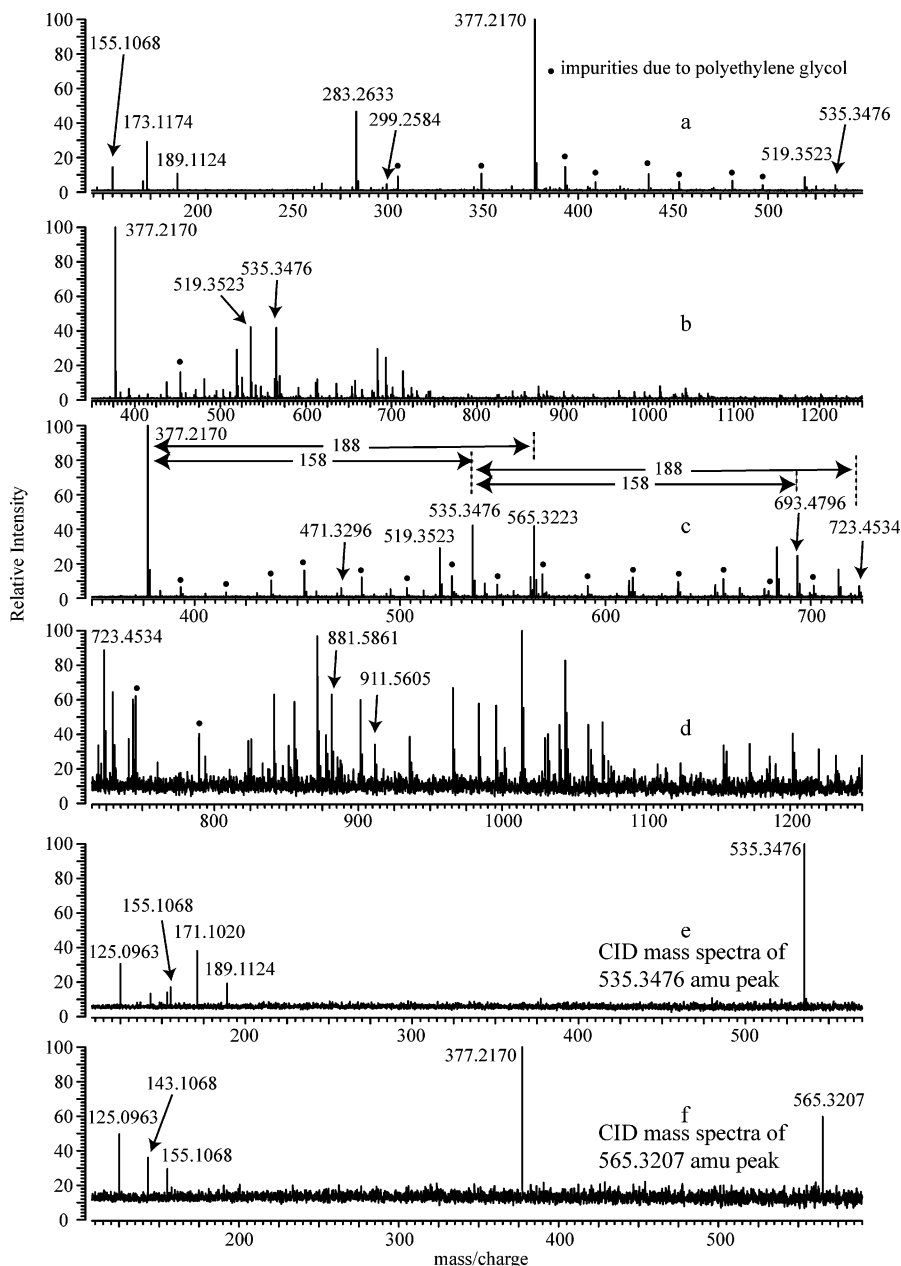
J. Phys. Chem. A, Vol. 111, No. 4, 2007 **625**

Figure 5. FT-MS spectra of products from the oxidation of oleic acid by ozone. (a) Mass spectra of low mass species. (b) Mass spectra with higher and wider mass range. (c) Zoom-in plot of Figure 5c for mass range of 350−725 amu. (d) Zoom-in plot of Figure 5c for mass range of 710−1250 amu. (e) CID mass spectra for peak of 535.3476 amu. (f) CID mass spectra for peak of 565.3207 amu. The peaks marked with solid circles (●) are the impurities in FT-MS due to standard chemical, polyethylene glycol, and the peaks without a mark and mass are unknown species. Conditions: 500 ppm O_3, 100 mL/min of air flow, 1 atm, 298 K, 87 ± 5% RH, and 30 μL of OL in 10 mL vial after 100 min O_3 exposure.

three azelaic acid molecules with one proton, or $C_{36}H_{69}O_4^+$, two oleic acid molecules with one proton. However, the peak at 565 amu is determined as 565.3223 amu shown in Figure 5c in high mass accuracy mass spectrometry. In a detailed calculation, the mass for $C_{36}H_{69}O_4^+$ is 565.5118 while the mass for $C_{27}H_{49}O_{12}^+$ is 565.3146, so the peak at 565.3223 amu is more likely to be $C_{27}H_{49}O_{12}^+$. As shown in Figure 5c, the mass spectra of oleic acid ozonolysis has a strong correlation with C9 species because the spacing between peaks is mainly correlated to 158 (nonanoic acid) or 188 (azelaic acid). For simplification, we assume the mass of each species is composed of the following species: nonanal (NN), 9-oxononanoic acid (OA), nonanoic acid (NA), azelaic acid (AA), and oleic acid (OL). In such a case, the mass spectra in Figure 5 can be summarized into C9, C18, C27, C36, and C45 species as shown in Table 2. The C9 species such as OA and AA are well-known

TABLE 2: Correlation of the Mass Spectra with the C9 Species and OL

| *m/z* ratio	chemical formula	no. of composed C9 species and OL {NN, OA, NA, AA, OL} + H$^+$
173.1174	$C_9H_{17}O_3^+$	{0, 1, 0, 0, 0}
189.1124	$C_9H_{17}O_4^+$	{0, 0, 0, 1, 0}
283.2633	$C_{18}H_{35}O_2^+$	{0, 0, 0, 0, 1}
299.2584	$C_{18}H_{35}O_3^+$	
377.2170	$C_{18}H_{33}O_8^+$	{0, 0, 0, 2, 0}
471.3696	$C_{27}H_{51}O_6^+$	{0, 0, 0, 1, 1}
519.3523	$C_{27}H_{51}O_9^+$	{0, 1, 1, 1, 0} or {1, 0, 0, 2, 0}
535.3476	$C_{27}H_{51}O_{10}^+$	{0, 0, 1, 2, 0}
565.3223	$C_{27}H_{49}O_{12}^+$	{0, 0, 0, 3, 0}
693.4796	$C_{36}H_{69}O_{12}^+$	{0, 0, 2, 2, 0}
723.4534	$C_{36}H_{67}O_{14}^+$	{0, 0, 1, 3, 0}
881.5861	$C_{45}H_{85}O_{16}^+$	{0, 0, 2, 3, 0}
911.5605	$C_{45}H_{83}O_{18}^+$	{0, 0, 1, 4, 0}
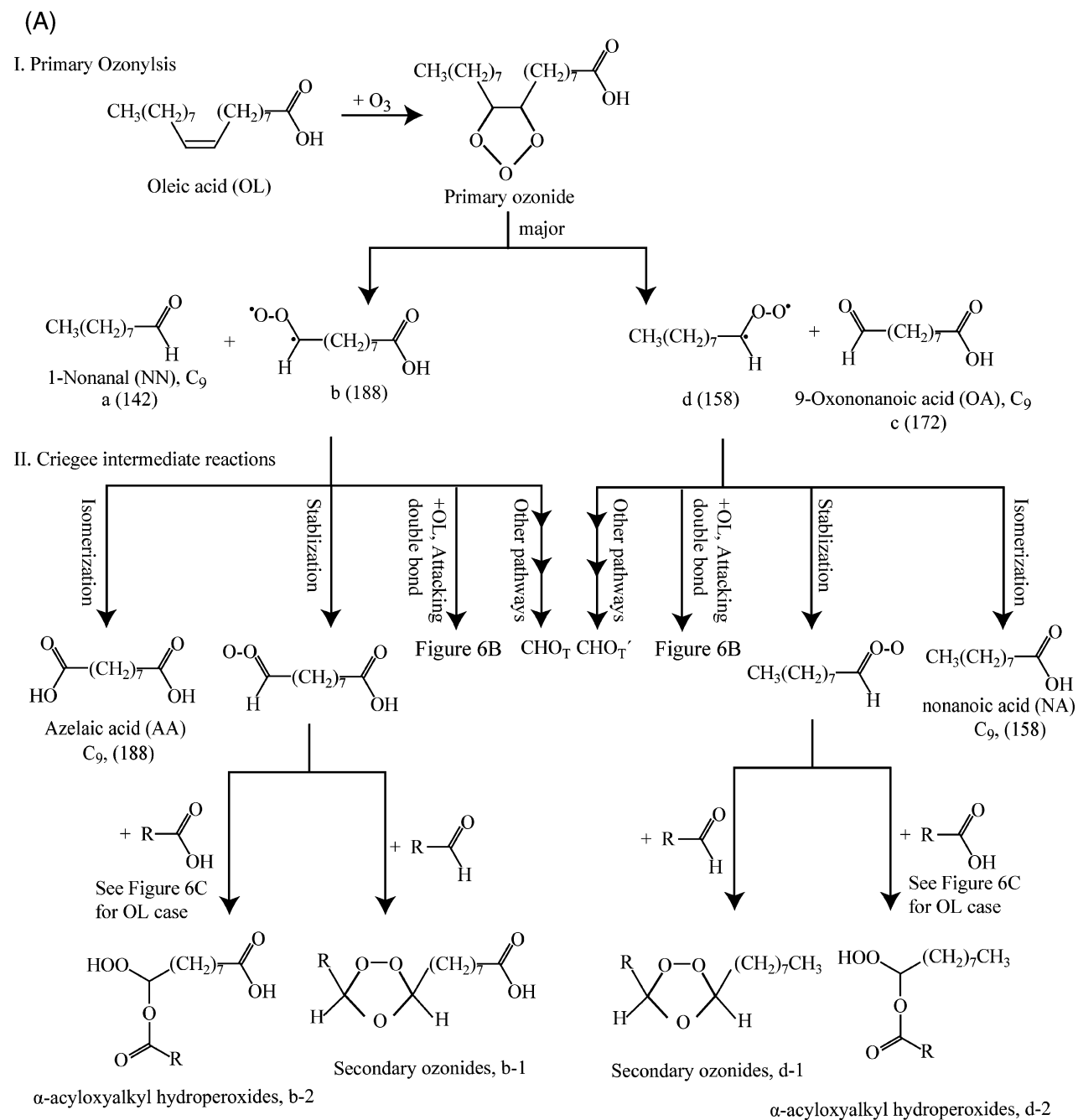
Figure 6. Proposed mechanism for the mass species identified in FT-ICR-MS. (A) C9 products and C9 Criegee intermediates reacting with aldehydes and carboxylic acids.

products from oleic acid ozonolysis, so this section will only focus on the high-mass species.

There are three C18 species observed in the FT-MS: $C_{18}H_{35}O_2^+$ (283.2633 amu), $C_{18}H_{35}O_3^+$ (299.2584 amu), and $C_{18}H_{33}O_8^+$ (377.217 amu). $C_{18}H_{35}O_2^+$ is the peak of protonated oleic acid and only present when the oxidation reaction is not completed. $C_{18}H_{35}O_3^+$ (299.2584 amu) is protonated 9-oxooctodecanoic acid or/and 10-oxooctodecanoic acid, which are the products from the reaction of C9-Criegee intermediate attacking the double bond of oleic acid with the mechanism shown in Figure 6B proposed and also observed by Zahardis et al.[25] $C_{18}H_{33}O_8^+$ in Table 2 is composed of one proton with two azelaic acid molecules, which can be the dimer of azaleic acid or other chemical forms. However, the CID mass spectra of peak 377.217 amu show no significant evidence of dimer (189 amu peak, protonated azelaic acid, is not significant; spectrum not shown). This result suggests that the 377.217 amu peak is

more likely to be a diperoxide or α-acyloxyalkyl hydroperoxide. In this study, the possibility of diperoxide can be excluded because it is less stable and likely decomposes into two 9-oxononanoic acid when the temperature is higher than 0 °C.[20,35] This concludes that the peak at 377.217 amu is likely a α-acyloxyalkyl hydroperoxide which is produced via two pathways: (1) the C9 Criegee intermediate (b in Figure 6A) attacking the carboxylic group of azelaic acid formed from the isomerization of C9 Criegee intermediate (b in Figure 6A) and (2) the isomerization of a C18 Criegee intermediate which is first generated by a C9 Criegee intermediate (b in Figure 6A) reacting with the matrix, oleic acid and then the double bond of such species is broken up by ozone (the pathway for g in Figure 6C). The C27 peak at 471.3296 amu, composed by one AA with one OL and only present when there is residual OL, supports the possibility of the C9 Criegee intermediates attacking
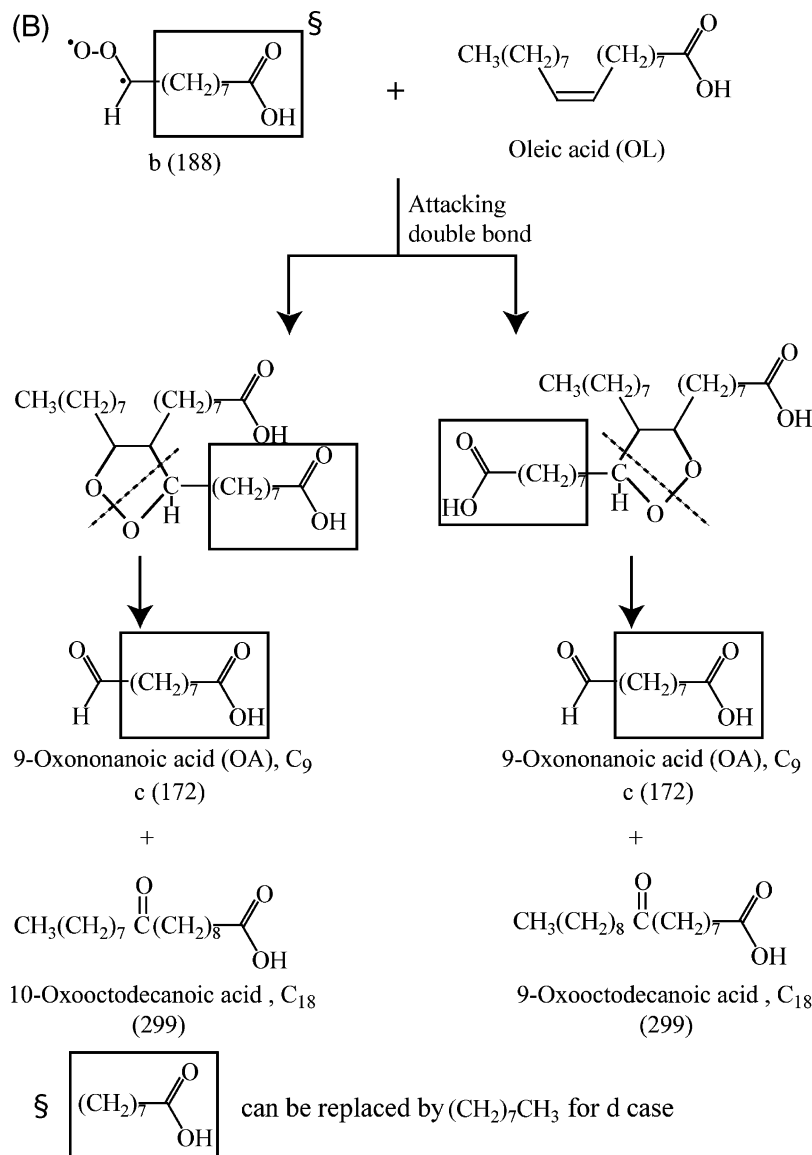
Oxidation of OL/NaCl(aq) Mixture Droplets with Ozone

J. Phys. Chem. A, Vol. 111, No. 4, 2007 **627**

Figure 6. Continued. (B) Possible mechanism for the 299 amu products: C9 Criegee intermediates attacking the double bond of oleic acid.

the carboxylic groups of oleic acid (b-2 in Figure 6B). Similar type products but dehydrated were reported by Zahardis et al.[25]

In addition to the peak at 471.3296 amu, three additional C27 species are identified in this study. The C27 peak at 519.3523 amu has the chemical formula $C_{27}H_{51}O_9^+$ which can have two types of combination as follows: (1) a secondary ozonide or α-acyloxyalkyl hydroperoxide composed by one proton with one OA, one NA, and one AA and (2) a secondary ozonide composed by one proton with one NN and two AA. The other two C27 peaks at 535.3476 and 565.3223 amu, C36, and C45 have major composing units of NA and AA which are minor products according the GC-MS and aerosol mass spectrometry (AMS) analysis.[14,26] The CID spectra in Figure 5e and 5f show the correlation of the 535.3476 amu product with AA (189.1124 amu) and 565.3223 amu product with a C18 α-acyloxyalkyl hydroperoxide (377.2170 amu), respectively. The C27 peak at 535.3476 amu can become C36 at 693.4796 amu by adding one NA or it can become C36 at 723.4534 amu by adding one AA. The link for C27 at 565.3223 amu to C36 is addition of NA to form C36 at 723.4534 amu. A similar trend is also applied for the transition of C36 to C45. Such results indicate that the high-mass products from the ozonolysis of oleic acid are mainly contributed from the stabilized Criegee intermediates, which are

usually isomerized into AA or NA in the gas-phase reactions. If we assume that reaction of stabilized Criegee intermediates with OL, OA, NA, and AA is competitive and the products have similar ionization efficiency in the FT-ICR-MS, it is likely that the high-mass species are generated by reaction of the stabilized Criegee intermediates with oleic acid via the mechanism shown in Figure 6C because there is no significant OA unit in the high-mass species. The mechanism for the propagation reaction observed in this study can be simplified as shown in Scheme 1, where CI is Criegee intermediate, AAHP is α-acyloxyalkyl hydroperoxide, and the underlined species are identified products in FT-ICR-MS. There are also other pathways such as the stabilized Criegee intermediates attacking the double bond of OL. In this study, we obtained 9-oxooctodecanoic or 10-oxooctodecanoic, which are the products of C9-stabilized Criegee intermediates attacking the double bond of oleic acid via the mechanism shown in Figure 6B. In Table 2 the maximum number of NA units in the high-mass species is two. This is due to the fact that propagation of stabilized Criegee intermediates with carboxylic groups is extendable for the OL and AA cases and terminated by the NA case.[14] The highest mass species we can resolve in this study is a C45 with a mass-
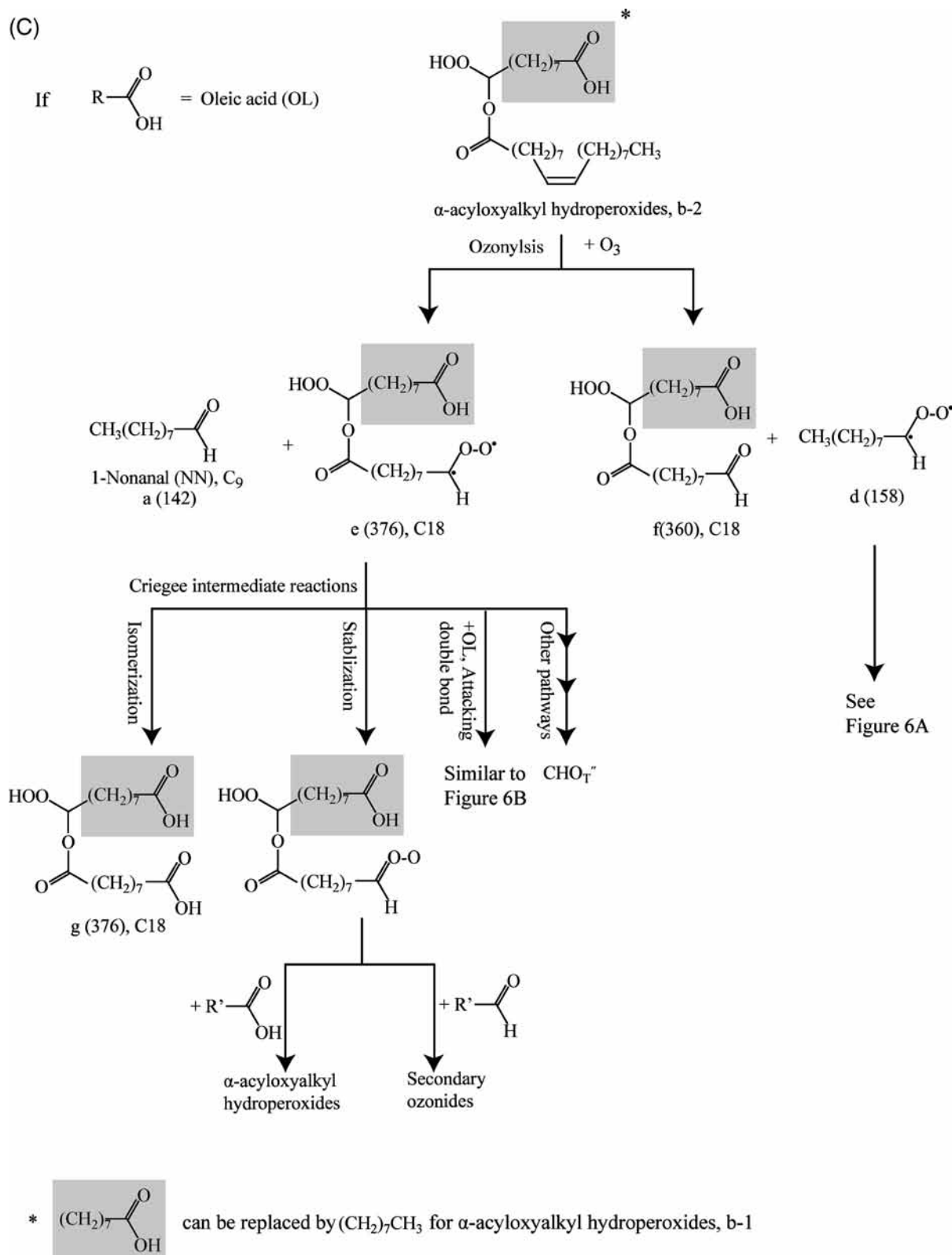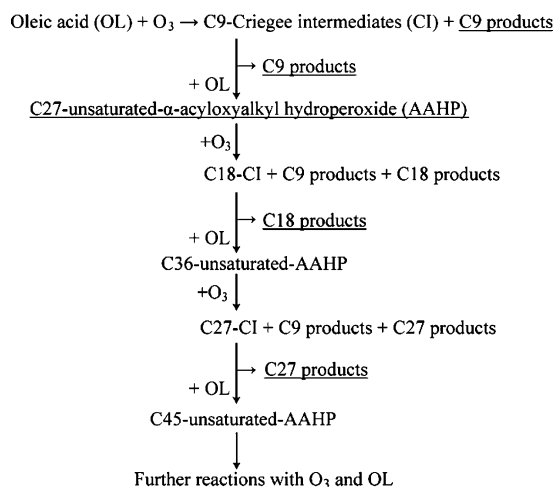
Figure 6. Continued. (C) Further propagation reactions when RCOOH is OL. CHO_T, CHO_T′, and CHO_T″ are products formed by other pathways as proposed by Katrib et al.[26]

to-charge ratio of 911.5605 amu. The formula for this mass is $C_{45}H_{83}O_{18}^+$, which is composed by one NA, three AA, and one proton.

Comparing this study with a previous study by Hung et al.,[14] only four peaks are found in common, 173, 189, 377, and 535 amu. The 378 amu observed by Hung et al. might correspond to the 377 amu peak in this study. The difference between the

two studies might be due to the sensitivity difference of products to the liquid-chromatography column and instruments. As compared to other studies,[20,24,25] this study shows evidence for propagation of α-acyloxyalkyl hydroperoxides initialized by the C9-stabilized Criegee intermediates attacking the carboxylic group of oleic acid and 9-oxooctodecanoic or 10-oxooctode-canoic, which are the products of C9-stabilized Criegee

Oxidation of OL/NaCl(aq) Mixture Droplets with Ozone

J. Phys. Chem. A, Vol. 111, No. 4, 2007 **629**

SCHEME 1

Oleic acid (OL) + O₃ → C9-Criegee intermediates (CI) + <u>C9 products</u>

      → <u>C9 products</u>
  + OL ⌐
<u>C27-unsaturated-α-acyloxyalkyl hydroperoxide (AAHP)</u>

    +O₃ ⌐
     C18-CI + C9 products + C18 products

      → <u>C18 products</u>
  + OL ⌐
  C36-unsaturated-AAHP

    +O₃ ⌐
     C27-CI + C9 products + C27 products

      → <u>C27 products</u>
  + OL ⌐
  C45-unsaturated-AAHP

     ↓

   Further reactions with O₃ and OL

intermediates attacking the double bond of oleic acid. However, the mass spectra of this study show low yield of secondary ozonides in the aerosol phase products and less OA associated with the α-acyloxyalkyl hydroperoxide species. It is possible that due to the efficiency difference in both vaporization and ionization processes from the analytical methods the volatile species will vaporize in the electrospray ionization process and not be detected in FT-ICR-MS while the high-mass products might not have significant vapor pressure in the thermal vaporization process to show signals over the detector. The possibility of different product yields between submicrometer particles and millimeter-sized droplets should not be excluded either. Further study might be needed to investigate the issue of products difference in different set ups and analytical methods.

3.4. Ozone Uptake in the Process of the Ozonolysis of Oleic Acid. The ozone absorbance at 254 nm as a function of time is shown in Figure 7 for three cases: (1) ATR cell with no droplets at RH = 10 ± 3%, (2) ATR cell with aqueous NaCl droplets at RH = 87 ± 5%, and (3) ATR cell with oleic acid droplets at RH = 10 ± 3%. The ozone inlet concentration is 500 ppm, and the time scale is relative. The variation of RH and presence of NaCl(aq) show no significant effect on the ozone temporal profiles. This phenomenon suggests that the effect of RH and liquid water on ozone uptake is negligible in this study. In Figure 7a depletion of the ozone absorbance as the flow passes through the ATR cell without droplets is due to the absence of ozone in the cell initially and possible ozone uptake by the wall. The ozone uptake by the wall of the cell and tubing is assumed to be negligible in this study because the ozone absorbance from the modeling, without uptake by the wall, is consistent with the measurement as described in the following section.

With the volume calibration of the ATR cell and tubing and subtracting the area below the inlet concentration of Figure 7a from Figure 7c, the amount of ozone consumed by oleic acid as the flow passing through the ATR cell direction is (1.5 ± 0.1) × 10⁻⁶ mol, which represents only 30 ± 2% of total oleic acid applied on the Ge crystal. These results indicate that oleic acid in the droplets is oxidized not only by ozone but also by other intermediates as suggested in the literature.[13,14,20,26] For example, the Criegee intermediates produced by addition of ozone to the double bond can further react not only with carboxylic acids but also with the double bond of oleic acid. The product identification from FT-ICR-MS provides qualitative evidence for both pathways. Hearn et al.[13] estimated that approximately 36% of oleic acid is consumed by reaction of
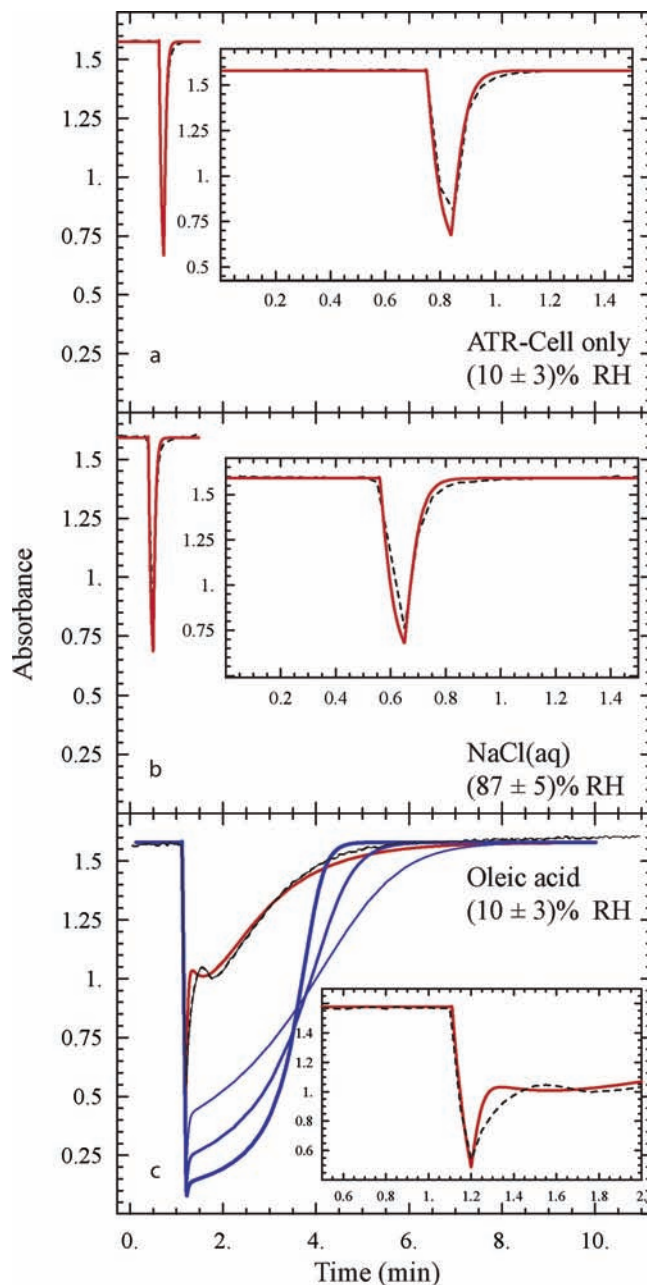

Figure 7. Temporal response for zone absorbance at 254 nm (black lines) and simulation results (red and blue lines) for three cases: (a) ATR cell only at 10 ± 3% RH, (b) NaCl(aq) droplets at RH = 87 ± 5%, and (c) oleic acid droplets at RH = 10 ± 3% with blue lines fitted by considering reaction 9 only. The blue lines correspond to k_a = 400, 800, and 1600 M⁻¹ s⁻¹ from thin to thick lines. The parameters for the red line are explained in the content. Conditions: 500 ppm O₃, 100 mL/min of air flow, 1 atm, 298 K, and 2.7 mm droplets.

stabilized Criegee intermediates with the carboxylic group of oleic acid. In this study, if we assume the double bonds of OL are either attacked by ozone or other secondary reactions, then we can estimate that approximately 70 ± 2% of oleic acid is consumed by secondary reactions, which is expected to be higher than in the literature.[13] In order to understand how the oxidation mechanism affects the ozone temporal profile, a kinetic model is established to simulate the ozone absorbance recorded at λ = 254 nm from UV−vis spectrometry.

3.4.1. Model Results. With the methodology described in section 2.4, the ozone partial pressure in the UV−vis cell is simulated. In order to compare the model results with the observation, the unit of ozone concentration is converted into

absorbance intensity via the absorbance cross-section of ozone at 254 nm. For ATR cell without droplets, there is no ozone uptake by oxidation reaction, so the observed ozone absorbance can be calculated based on the parameters in Table 1. The good agreement between the modeled profile and the measurement in Figure 7a supports the assumption of ignorance of the ozone uptake by the wall. For NaCl aqueous droplets, ozone can diffuse into the droplets and react with chloride ion via reaction 6. However, the rate constant for reaction 6 is less than 3×10^{-3} M^{-1} s^{-1}, which might not be detectable in this study. The model outcomes with or without considering the oxidation reaction between NaCl and ozone are indistinguishable, and both agree well with the measurement shown in Figure 7b. Even though the slow reaction of ozone with chloride does not reveal a significant loss of ozone, it does change the hygroscopicity of the droplets significantly as described in section 3.2.

Unlike the NaCl(aq) case, oxidation of oleic acid with ozone significantly changes the ozone temporal profile, as shown in Figure 7c. Reaction of oleic acid is initialized by addition of ozone to the double bond. As suggested by Hearn et al.,[13] reaction of oleic acid with ozone is a surface reaction but can be illustrated by an exponential equation. In this study, the reaction limiting parameters are not determined but the reaction is assumed to be resolved by an exponential function for OL. The rate constant obtained from variation of organic IR spectra might contain the information of other parameters such as the rate constant of surface reaction and the thickness of the surface layer as described by Hearn et al.[13] In order to simulate the ozone temporal profile, two mechanisms are taken into account: with and without secondary reactions. Without secondary reactions, ozone is taken up by the following reaction only
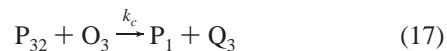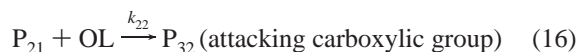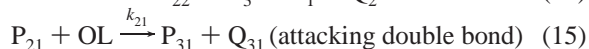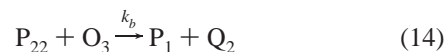
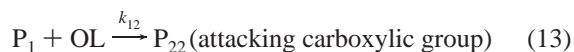$$OL + O_3 \xrightarrow{k_a} P_1 + Q_1 \qquad (9)$$
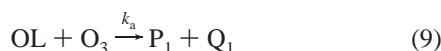
Oleic acid (OL) is oxidized by ozone with a rate constant of k_a to generate Criegee intermediates (P_1) and stable compounds (Q_1). Equation 2 is then updated with reaction 9 into two equations as follows

$$\frac{dP_{O3,2}[t]}{dt} = \frac{v_f}{V_2}(P_{O3,1}[t] - P_{O3,2}[t]) - P_{O3,2}[t]Hk_a\, OL[t]\left(\frac{v_d}{V_2}RT\right) \qquad (10)$$

$$\frac{dOL[t]}{dt} = -k_a P_{O3,2}[t]H\, OL[t] \qquad (11)$$

where H is Henry's law constant of ozone and 0.1 M/atm in this calculation, $OL[t]$ is the concentration of oleic acid as a function of time and is 3.16 M when $t = 0$ min, and $((v_d/V_2)RT)$ is a term to convert the concentration of ozone in droplets into partial pressure with v_d as the total volume of droplets, R as the gas constant, and T as the temperature. In eq 10 there is only a variable parameter, k_a. For a given k_a value, the ozone concentration can be obtained by solving the differential eqs 1−4. In Figure 7c three k_a values are applied to calculate the simulated ozone temporal profile to the measurement, but the results (blue lines) are not satisfied. In the following case the secondary reactions of the stabilized Criegee intermediates attacking oleic acid via the carboxylic group and double bond are included in addition to reaction 9 to improve the simulation

$$P_1 + OL \xrightarrow{k_{11}} P_{21} + Q_{21} \text{ (attacking double bond)} \qquad (12)$$

$$P_1 + OL \xrightarrow{k_{12}} P_{22} \text{(attacking carboxylic group)} \qquad (13)$$

$$P_{22} + O_3 \xrightarrow{k_b} P_1 + Q_2 \qquad (14)$$

$$P_{21} + OL \xrightarrow{k_{21}} P_{31} + Q_{31} \text{ (attacking double bond)} \qquad (15)$$

$$P_{21} + OL \xrightarrow{k_{22}} P_{32} \text{ (attacking carboxylic group)} \qquad (16)$$

$$P_{32} + O_3 \xrightarrow{k_c} P_1 + Q_3 \qquad (17)$$

In this case, P_1 can further react with oleic acid by either attacking the double bonds to form other active intermediates (P_{21}) and other stable products of Q_{21} or attacking the carboxylic group to form α-acyloxyalkyl hydroperoxides (P_{22}) which may be further oxidized by O_3 to form Criegee intermediates (which is assumed to be as the same as P_1 to simplify the kinetics in this study) and stable products (Q_2). P_{21} is assumed to have similar ability as P_1 to react with oleic acid in two pathways. In sequence, P_{31} is similar to P_{21} but the further reaction is assumed negligible at this simple model. With consideration of reactions of 9 and 12−17, eq 2 is then updated for different chemical composition into the following equations

$$\frac{dP_{O3,2}[t]}{dt} = \frac{v_f}{V_2}(P_{O3,1}[t] - P_{O3,2}[t]) - P_{O3,2}[t]H(k_a\, OL[t] + k_b P_{22}[t] + k_c P_{32}[t])\left(\frac{v_d}{V_2}RT\right) \qquad (18)$$

$$\frac{dOL[t]}{dt} = -(P_{O3,2}[t]Hk_a + P_1(k_{11} + k_{12}) + P_{21}(k_{21} + k_{22}))\, OL[t] \qquad (19)$$

$$\frac{dP_1[t]}{dt} = P_{O3,2}[t]H(k_a\, OL[t] + k_b P_{22}[t] + k_c P_{32}[t]) - P_1(k_{11} + k_{12})\, OL[t] \qquad (20)$$

$$\frac{dP_{21}[t]}{dt} = (k_{11}P_1[t] - k_{21}P_{21}[t] - k_{22}P_{21}[t])\, OL[t] \qquad (21)$$

$$\frac{dP_{22}[t]}{dt} = k_{11}P_1\, OL[t] - k_b P_{22}[t]P_{O3,2}[t]H \qquad (22)$$

$$\frac{dP_{32}[t]}{dt} = k_{22}P_{21}\, OL[t] - k_c P_{32}[t]P_{O3,2}[t]H \qquad (23)$$

For a set of parameters the differential equations can be solved numerically to obtain the individual concentration as a function of time. The red line in Figure 7c with parameters of $k_a = 58 \pm 3$ M^{-1} s^{-1}, $k_{11} \approx k_{12} > 0.01$ M^{-1} s^{-1}, $k_{21} \geq 1$ M^{-1} s^{-1}, $k_{22} = 0.15$ M^{-1} s^{-1}, and $k_b = 2880$ M^{-1} s^{-1} agrees well with the measurement. The simulated curve is not sensitive to k_c, and this is possibly due to the low concentration of P_{32}. In order to compare with the rate constant obtained from IR spectra variation, k_a is convert to different units by this equation: $k_{a'} = k_a \times H \times P_{O3} = 0.17 \pm 0.01$ min^{-1}, which is less than the rate constant obtained from IR spectra, 0.5 ± 0.1 min^{-1} for 500 ppm O_3. The rate constant is estimated to be 0.023 ± 0.002 min^{-1} for 20 ppm O_3 as shown in Figure 3.

3.4.2. Comparison with Other Studies. In order to compare this study with the literature, the uptake coefficient (γ) is

Oxidation of OL/NaCl(aq) Mixture Droplets with Ozone

J. Phys. Chem. A, Vol. 111, No. 4, 2007 **631**

estimated based on the following equation[13]

$$\frac{d[OL]}{dt} = -\gamma\left(\frac{P_{O3}\bar{c}}{4RT}\right)\frac{S_A}{V} \tag{24}$$

where $\bar{c}$ (360 m s^{-1}) is the mean speed of O$_3$ molecules and S_A/V is the surface area-to-volume ratio (1.5 × 10^4 m^{-1} in this study). The uptake coefficients in the current study are reported in two ways: the spectra variation of organic species and the ozone concentration simulation. The uptake coefficient is estimated to be (1.1 ± 0.2) × 10^{-3} for 20 ppm O$_3$ and (9.5 ± 2.0) × 10^{-4} for 500 ppm O$_3$ from the rate constants measured from the IR spectra, which can be used to represent OL oxidation rate[14] and (3.2 ± 0.5) × 10^{-4} calculated based on k_a for 500 ppm O$_3$. The γ value obtained from the ozone temporal profile is only one-third of that from IR measurement of organic species. These results are consistent with the literature: the uptake coefficients estimated from the decay of O$_3$ on flow tubes coated with oleic acid[16,19,27] are usually smaller than the values obtained from the decay of oleic acid.[18,28] The higher uptake coefficient obtained from the loss of oleic acid is expected because the overall oleic acid rate is a combination of ozone oxidation and secondary reactions. The secondary reactions of the stabilized Criegee intermediates with oleic acid, especially reaction with the double bond, which is assumed negligible in other studies, appear to be important and comparable with the reaction with the carboxylic group ($k_{11} \approx k_{12}$). As compared with other studies reporting ozone uptake by measuring ozone concentration,[16,19,27] the initial ozone uptake coefficient by oleic acid estimated from ozone temporal profiles in this study is also much less, (3.2 ± 0.5) × 10^{-4} vs 8 × 10^{-4}. This difference might be due to the different physical shape of OL (droplets vs films) and experimental environment (vacuumed vs 1 atm). This study implies the importance of secondary reactions such as the stabilized Criegee intermediates reacting with oleic acid via both the carboxylic group and the double bond, which has been proposed previously by Katrib et al.[26]

4. Conclusions

In this study, the temporal profiles of organic IR absorbance and ozone UV absorbance were monitored in real time simultaneously to investigate the oxidation kinetics while the high-mass species were analyzed by highresolution and high mass accuracy FT-ICR-MS. The increased absorbance of water bending peak ($\nu = 1630$ cm^{-1}) at RH = 87 ± 5% suggests that the hygroscopicity of the OL droplets changes after exposure to ozone. The deposited liquid water might change the chemical reactivity of the droplets. As to the internal mixture OL/NaCl-(aq) droplets, the overall liquid water content decreases as the mixture droplets exposure to enough ozone at RH = 87 ± 5%. This result indicates that the hygroscopicity of such mixture droplets is complex and can vary in the course of the oxidation reactions. Furthermore, if the size of the particles decreases due to the decreasing liquid water content, the oxidation reaction of OL in OL/NaCL(aq) particles might reduce the particle size and reduce the aerosol direct forcing for the case presented in this study. However, if RH is high enough, leading to deliquescence of the whole particle, the effect of the oxidation might indeed be in the opposite.

FT-ICR-MS analysis led to identification of several C18, C27, C36, and C45 products. Our results suggest that the propagation reaction is possibly initiated by the stabilized Criegee intermediates reacting with oleic acid because identified products were predominantly composed of nananoic acid and azelaic acid,

which were found as minor products. With the real-time monitoring ozone concentration by UV−vis spectrometry, the ozone consumed by OL oxidation is estimated to be only 30 ± 2% of OL. The temporal response of ozone absorbance can only be well simulated when the secondary reactions are included. The ozone uptake coefficient on OL is estimated to be (3.2 ± 0.5) × 10^{-4} from simulation for 500 ppm O$_3$ and is lower compared to that from the IR spectra variation and other studies. The overall results indicate the importance of secondary reactions, which can contribute to the discrepancy among uptake coefficients obtained from different studies.

Ozone and oleic acid in this study are at higher concentrations compared to atmospheric conditions. However, the similar ozone uptake coefficient between this oleic acid droplet case with high ozone concentration and other oleic acid aerosol cases[13,18,28] with low ozone concentration suggests that the results of this study might be interpolated to atmospheric conditions and provide information related to the physiochemical properties and mechanism in the ozonolysis of oleic acid aerosol. With the uptake coefficient of (1.1 ± 0.2) × 10^{-3} at 20 ppm O$_3$, the lifetime (decreasing to 1/e of its initial concentration) of pure oleic acid aerosol at a diameter of 60 nm is then estimated to be 2 min at 100 ppb ozone. However, such a short lifetime is not consistent with field measurements, as also stated in other studies.[24,27,36] Other effects such as the physical phase and composition of aerosols might play important roles.[24,27,36] Further study on the influence of ozone and oleic acid concentrations on both kinetics and products yields is required to properly link the laboratory data with the atmospheric system.

References and Notes

(1) Novakov, T.; Penner, J. E. *Nature* **1993**, *365*, 823.

(2) Seinfeld, J. H.; Pandis, S. N. *Atmospheric Chemistry and Physics*; Wiley: New York, 1998.

(3) Kanakidou, M.; Seinfeld, J. H.; Pandis, S. N.; Barnes, I.; Dentener, F. J.; Facchini, M. C.; Van Dingenen, R.; Ervens, B.; Nenes, A.; Nielsen, C. J.; Swietlicki, E.; Putaud, J. P.; Balkanski, Y.; Fuzzi, S.; Horth, J.; Moortgat, G. K.; Winterhalter, R.; Myhre, C. E. L.; Tsigaridis, K.; Vignati, E.; Stephanou, E. G.; Wilson, J. *Atmos. Chem. Phys.* **2005**, *5*, 1053.

(4) Eliason, T. L.; Gilman, J. B.; Vaida, V. *Atmos. Environ.* **2004**, *38*, 1367.

(5) Molina, M. J.; Ivanov, A. V.; Trakhtenberg, S.; Molina, L. T. *Geophys. Res. Lett.* **2004**, *31*.

(6) Bertram, A. K.; Ivanov, A. V.; Hunter, M.; Molina, L. T.; Molina, M. J. *J. Phys. Chem. A* **2001**, *105*, 9415.

(7) Stephanou, E. G.; Stratigakis, N. *Environ. Sci. Technol.* **1993**, *27*, 1403.

(8) Rinehart, L. R.; Fujita, E. M.; Chow, J. C.; Magliano, K.; Zielinska, B. *Atmos. Environ.* **2006**, *40*, 290.

(9) Kawamura, K.; Ishimura, Y.; Yamazaki, K. *Glob. Biogeochem. Cycle* **2003**, *17*.

(10) Schauer, J. J.; Rogge, W. F.; Hildemann, L. M.; Mazurek, M. A.; Cass, G. R. *Atmos. Environ.* **1996**, *30*, 3837.

(11) Rogge, W. F.; Hildemann, L. M.; Mazurek, M. A.; Cass, G. R.; Simonelt, B. R. T. *Environ. Sci. Technol.* **1991**, *25*, 1112.

(12) Gill, P. S.; Graedel, T. E.; Weschler, C. *J. Rev. Geophys.* **1983**, *21*, 903.

(13) Hearn, J. D.; Lovett, A. J.; Smith, G. D. *Phys. Chem. Chem. Phys.* **2005**, *7*, 501.

(14) Hung, H. M.; Katrib, Y.; Martin, S. T. *J. Phys. Chem. A* **2005**, *109*, 4517.

(15) Katrib, Y.; Martin, S. T.; Rudich, Y.; Davidovits, P.; Jayne, J. T.; Worsnop, D. R. *Atmos. Chem. Phys.* **2005**, *5*, 275.

(16) Moise, T.; Rudich, Y. *J. Phys. Chem. A* **2002**, *106*, 6469.

(17) Smith, G. D.; Woods, E.; Baer, T.; Miller, R. E. *J. Phys. Chem. A* **2003**, *107*, 9582.

(18) Smith, G. D.; Woods, I. E.; DeForest, C. L.; Baer, T.; Miller, R. E. *J. Phys. Chem. A* **2002**, *106*, 8085.

(19) Thornberry, T.; Abbatt, J. P. D. *Phys. Chem. Chem. Phys.* **2004**, *6*, 84.

(20) Ziemann, P. J. *Faraday Discuss.* **2005**, *130*, 469.

(21) Broekhuizen, K. E.; Thornberry, T.; Kumar, P. P.; Abbatt, J. P. D. *J. Geophys. Res.-Atmos.* **2004**, *109*, Dec 21.

(22) Asad, A.; Mmereki, B. T.; Donaldson, D. J. *Atmos. Chem. Phys.* **2004**, *4*, 2083.

(23) Seinfeld, J. H.; Pankow, J. F. *Annu. Rev. Phys. Chem.* **2003**, *54*, 121.

(24) Katrib, Y.; Biskos, G.; Buseck, P. R.; Davidovits, P.; Jayne, J. T.; Mochida, M.; Wise, M. E.; Worsnop, D. R.; Martin, S. T. *J. Phys. Chem. A* **2005**, *109*, 10910.

(25) Zahardis, J.; LaFranchi, B. W.; Petrucci, G. A. *Atmos. Environ.* **2006**, *40*, 1661.

(26) Katrib, Y.; Martin, S. T.; Hung, H. M.; Rudich, Y.; Zhang, H.; Slowik, J. G.; Davidovits, P.; Jayne, J. T.; Worsnop, D. R. *J. Phys. Chem. A* **2004**, *108*, 6686.

(27) Knopf, D. A.; Anthony, L. M.; Bertram, A. K. *J. Phys. Chem. A* **2005**, *109*, 5579.

(28) Morris, J. W.; Davidovits, P.; Jayne, J. T.; Jiménez, J. L.; Shi, Q.; Kolb, C. E.; Worsnop, D. R.; Barney, W. S.; Cass, G. *Geophys. Res. Lett.* **2002**, *29*, 1357.

(29) Blanchard, D. C. *Science* **1964**, *146*, 396.

(30) Ellison, G. B.; Tuck, A. F.; Vaida, V. *J. Geophys. Res.-Atmos.* **1999**, *104*, 11633.

(31) King, M. D.; Thompson, K. C.; Ward, A. D. *J. Am. Chem. Soc.* **2004**, *126*, 16710.

(32) Hearn, J. D.; Smith, G. D. *J. Phys. Chem. A* **2004**, *108*, 10019.

(33) Finlayson-Pitts, B. J. *Chem. Rev.* **2003**, *103*, 4801.

(34) Johnsson, K.; Engdahl, A.; Ouis, P.; Nelander, B. *J. Phys. Chem.* **1992**, *96*, 5778.

(35) Fliszar, S.; Chylinsk, Jb. *Can. J. Chem.* **1968**, *46*, 783.

(36) Worsnop, D. R.; Morris, J. W.; Shi, Q.; Davidovits, P.; Kolb, C. E. *Geophys. Res. Lett.* **2002**, *29*.